JOURNAL OF PROPULSION AND POWER
Vol. 20, No. 4, July–August 2004

Plasma Characterization of a 10-cm Diameter Microwave Discharge Ion Thruster

Ikkoh Funaki,* Hitoshi Kuninaka,† and Kyoichiro Toki‡
Institute of Space and Astronautical Science, Japan Aerospace Exploration Agency, Kanagawa 229-8510, Japan

Plasma characterization was conducted for an electron-cyclotron-resonance (ECR) type ion thruster. For a 10-cm diameter microwave discharge ion source consisting of two samarium cobalt magnet rings surrounding a centered waveguide for launching microwaves, plasma profiles were found to have severely non-uniform distributions, with localized plasma found near the magnet rings. This localized plasma is mainly produced in the magnetic flux tubes between the two ring magnets, where electrons gain microwave energy as they pass the ECR line during the bouncing movement between magnetic mirrors. To obtain a low-cost microwave ion source, this type of ionization mechanism can be exploited. When introducing microwaves through a low magnetic field boundary, however, it is impossible to eliminate the accessibility difficulty related to the cutoff density, which results in a plasma below the cutoff density. Because of the accessibility difficulty, in this work, only a relatively small ion beam current density of 1.8 mA/cm^2 was achieved.

Nomenclature

B	=	magnetic flux density, T
$B_{\max}$	=	maximum magnetic flux density along the mirror magnet, T
$B_{\min}$	=	minimum magnetic flux density along the mirror magnet, T
C	=	conductance of the perforated metal plate, sccm/Pa
e	=	electrical charge, 1.60×10^{-19} C
I_b	=	ion beam current, A
ℓ'	=	length of the magnetic flux tube, m
m_e	=	mass of electron, 9.11×10^{-31} kg
m_i	=	mass of xenon atom, 2.18×10^{-25} kg
$\dot{m}_i$	=	mass flow rate for ion source, sccm
$\dot{m}_{\text{neut}}$	=	mass flow rate for neutralizer, sccm
$\dot{m}_{\text{sim}}$	=	simulated mass flow rate, sccm
n_e	=	electron density, m^{-3}
P_f	=	input microwave power for ion source, W
P_{neut}	=	input microwave power for neutralizer, W
p_1	=	pressure inside the vacuum chamber, Pa
p_2	=	pressure inside the discharge chamber, Pa
r	=	radial position from the center line of the ion source, m
r_p	=	radius of probe, m
T_e	=	electron temperature, K
$u_{//}$	=	velocity along the magnetic field, m/s
$u_{\perp}$	=	velocity across the magnetic field, m/s
V_{ac}	=	accelerator voltage, V
V_f	=	floating potential, V
V_s	=	space potential, V
V_{sc}	=	screen voltage, V
V_{neut}	=	neutralizer voltage, V
W_{tot}	=	energy of electron, J, $W_{\text{tot}} = 1/2 m_e u_{//}^2 + \mu B$
x	=	coordinate, m
y	=	coordinate, m
z	=	coordinate, axial position from the decelerator grid of the ion thruster head, axial position from the perforated metal grid, m
η	=	propellant utilization efficiency, %
λ	=	mean free path, m
λ_D	=	Debye length, m
λ_g	=	wavelength in transmission circuit, m
μ	=	magnetic moment, J/T
ν_{ECR}	=	frequency of electron's energy gain by electron-cyclotron-resonance process, Hz
ν_{ee}	=	electron–electron collision frequency, Hz
ν_{ei}	=	electron–ion Coulomb collision frequency, Hz
ν_{en}	=	electron–atom collision frequency, Hz
τ_{bounce}	=	time for each bouncing motion of electron
ω	=	angular frequency of microwave, rad/s
ω_c	=	electron cyclotron frequency, rad/s
ω_p	=	plasma frequency, rad/s
ω_{UH}	=	upper hybrid resonant frequency, rad/s

I. Introduction

FOLLOWING dc- and rf-discharge technologies, microwave discharge is now considered to be the third plasma production principle that can be utilized for ion production in an ion engine system.[1] The first flight test of a microwave ion engine system started in 2003. Four 400-W thrusters are now being used as primary propulsion for a Japanese space probe exploring an asteroid.[2,3] The key feature of the microwave-driven system is its simplified architecture and the reduced number of components as compared to dc- and even rf-based systems. As shown in Fig. 1a, with the hollow cathode removed from the main discharge chamber the ion source is totally free from high-temperature components. Accordingly, a heater for starting up the hollow cathode and the corresponding power supply are not needed. Similarly, the neutralizer does not employ a hollow cathode, but instead uses a compact microwave discharge electron source, as shown in Fig. 1b. Both sources are powered by two separate 4.25-GHz microwave sources. For the ion source, impedance matching of the microwaves was made possible by selecting an appropriate geometry of the antenna-waveguide transformer. Accordingly, the ion source does not require any additional impedance-matching devices, which would lower the reflected microwave toward the power source. For the case of the neutralizer, a stub tuner was used to keep the reflected microwave below 0.5 W. Our approach in optimizing these microwave sources is to find the best operational condition, that is, combination of microwave power

Received 3 January 2002; revision received 19 August 2002; accepted for publication 2 September 2002.

*Associate Professor, Research Division for Space Transportation Engineering, 3-1-1 Yoshinodai, Sagamihara. Member AIAA.

†Associate Professor, Research Division for Space Transportation Engineering, 3-1-1 Yoshinodai, Sagamihara. Senior Member AIAA.

‡Professor, Research Division for Space Transportation Engineering, 3-1-1 Yoshinodai, Sagamihara. Member AIAA.

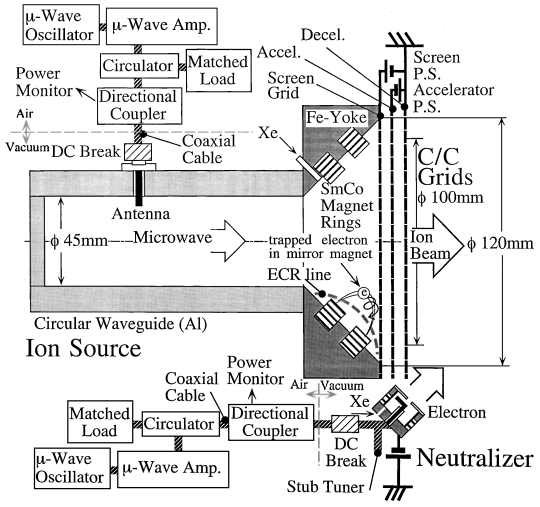

a)

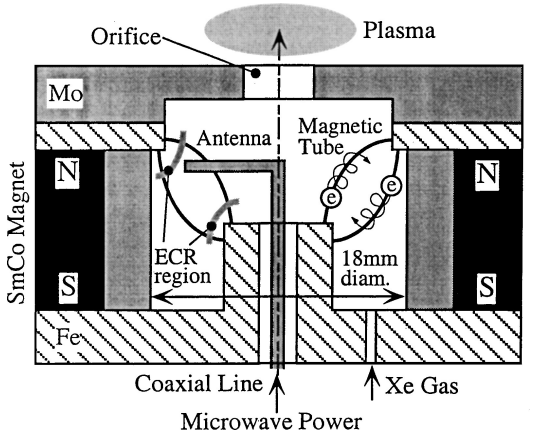

b)

Fig. 1 Schematics of microwave discharge ion thruster: a) ion thruster head and its electrical connections and b) neutralizer.

and mass flow rate for a given discharge chamber geometry. This type of optimization is essential because elimination of cathodes from the discharge chamber reduces the flexibility of the thruster to operate in a wide range of operational conditions. The optimal operational condition as determined by ground testing is nominally used for a single operational condition for the flight thruster. When an operation with reduced electrical power is required, the mass flow rate was decreased from this optimized value without changing the microwave power. With this fixed microwave power approach, there is no need to adjust tuning devices. Hence, employing a power divider our flight model adopted a thruster head with a single microwave power supply that powers both the ion source and the neutralizer.

Removal of the hollow cathode and related components drastically simplifies thruster startup. Plasma is easily ignited after xenon gas is introduced and the single microwave power supply system is switched on. It was confirmed that the use of a single microwave power supply system did not influence the ignition process of each source. In addition to the just-mentioned simple, hence robust, thruster head design consisting of only magnets, iron yokes, and aluminum body, the microwave power source is available off the shelf as a qualified system developed and tested for satellite communication.

To improve the performance of the microwave ion source, energy transfer to the plasma has to be maximized, and the discharge losses should be minimized. Among various microwave ion source designs, we incorporated and revised the microwave plasma generator design proposed by Goede, who introduced the microwave through a waveguide into a line-cusp discharge chamber made of samarium cobalt (SmCo) magnets and soft iron.[4] This design enhances the resonant microwave-to-plasma energy transfer mechanism, the so-called electron cyclotron resonance (ECR), in which magnetically trapped electrons resonantly absorb electric field oscillation perpendicular to the magnetic field, and energize its gyro motions.

The initial effort on the development of ECR-type ion thrusters at the Institute of Space and Astronautical Science started from 10-cm-diam laboratory model thrusters, whose discharge chamber had two or three SmCo magnet rings and iron yokes surrounding a centered waveguide for launching microwaves. Into this magnetic circuit, 5.9-GHz microwaves were launched from a centered waveguide, which is located coaxially to the ring magnets. After various discharge chamber configurations were studied, the thruster Yoshino-III (Y-III) achieved an ion production cost of 400 W/A and a propellant utilization efficiency of 60% for a 120-W microwave input power.[5] Using probe diagnostics, a plasma near the cutoff density of the microwave was confirmed in this discharge chamber.[6] The plasma production inside the discharge chamber was found to be localized to a region near the ECR zone, which is characterized by large negative floating potential, indicating a large number of electrons. Strong light emission, which corresponds to ionization collision by high energy electrons, was observed.[7–9] The discharge chamber configuration was further improved to enhance this ECR discharge using 4.2-GHz microwaves, and the 10-cm-diam chamber was scaled down to a low-power mode, 300-W (100-mA) class, achieving 300-W/A ion production cost and 85% propellant utilization efficiency for Y-IV thruster.[1,10] Based on this model, the first engineering model (EM) for MUSES-C was developed in 1997, producing a 140 mA beam current with an ion production cost 230 W/A and a propellant utilization efficiency of 88%, for 4.2-GHz microwave. Although the weights of the EM and the Y-IV are different, their magnetic field designs are almost the same. This paper describes studies of the microwave discharge plasmas for the EM and the Y-IV using Langmuir probe diagnostics. After a discussion of the microwave-to-plasma coupling of the ion source, the plasma of the microwave discharge neutralizer is characterized.

II. Design of Ion Thruster Head

A. Ion Source

Figure 1a shows a schematic of a microwave discharge ion thruster head. The ion source consists of a magnetic circuit, which has two ring magnets and iron yokes; these magnetic circuits as well as the aluminum body comprise the discharge chamber wall. After xenon gas is introduced into the discharge chamber, microwave power in the TE11 mode is injected using a circular wave guide. Plasma production relies heavily on a process of energizing electrons that are trapped in the magnetic tube between the two ring cusps. During the movement in the magnet mirror, the electrons are rotating at an angular frequency

$$\omega_c = eB/m_e \tag{1}$$

around the B-field. A resonant wave-particle interaction occurs when a microwave of frequency ω_c has a right hand circularly polarized electric field component in the plane perpendicular to B. When the electrons see this perpendicular wave component, the damping of the electromagnetic wave and corresponding collisionless ECR absorption lead to a resonant energy gain of the electron. As a result, the electron velocity component in the direction perpendicular to the B-field increases. For a bounded plasma device, however, it is usually impossible to establish a purely right-hand polarized wave; the electric field possesses a left circularly polarized component that does not directly contribute to ECR. Furthermore, for the small ion source adopted in this case, it is difficult to launch the wave along the B-field, so that the wave is introduced perpendicularly to the B-field in such forms as extraordinary or ordinary waves, both of which are considered to be of importance for the microwave ion engine. The details of microwave-plasma coupling will be discussed later.

After power absorption by an adequate wave-particle coupling channel, most of the energized particles will remain in the magnetic tube. To maintain the microwave discharge, trapped high-energy electrons above the ionization energy should collide with the background xenon atoms, and depleted high-energy electrons are continuously supplemented by successive injections of microwave power. The magnetic flux tube plays the role of producing and containing primary electrons, and hence it is called a virtual cathode. Once the microwave discharge is initiated, the plasma produced in the virtual cathode should be introduced toward the ion optics without significant losses to the walls. Here again the strong magnetic field works to suppress the ion wall losses, although, as one can easily imagine, the plasma production near the wall can result in large wall losses**.** This condition requires a large magnetic field as compared to dc-type ion thrusters.

Before the just-mentioned plasma can be successfully produced, the microwave transmission circuit should be tuned so as to enhance the microwave power absorption into the plasma. This procedure is called impedance matching because the plasma corresponds to a variable load at the end of a 50-Ω distributed circuit. A properly tuned system makes it possible for the nonabsorbed reflected waves to penetrate the plasma again and be partially absorbed. Through such a matching system, it is possible to reverse all of the reflected waves back to the discharge chamber, although some of this energy is tied up in the form of a standing wave between the discharge chamber and the tuner. If the length of this standing wave along the microwave circuit is too long, considerable power loss along the circuit is expected. This is prevented by minimizing the distance between the discharge chamber and the tuner. Thus, a compact tuning system that can confine the standing wave in a small discharge chamber is strongly preferred for the microwave ion engine. As shown in Fig. 1a, microwave power, which is originally transmitted via a coaxial cable, is converted into a circular waveguide, and then, by selecting the geometry of this convertor and the discharge chamber itself, it is possible to suppress most of the reflected wave and to optimize the plasma production. Because the axial length of the discharge chamber including the microwave launcher is about $2\lambda_g$, the system not only works as a microwave launcher but also helps to optimize the pattern of the standing wave inside the chamber. The optimization of the standing wave pattern is important because a large microwave oscillation near the ECR point apparently enhances plasma production. Note that the chamber geometry was optimized for both accelerated and nonaccelerated operation. The discharge chamber geometry of the ion source enables easy plasma ignition without employing any matching devices, and low-cost ion beam production is possible using the same discharge chamber configuration when the ion beam is extracted.

B. Neutralizer

As shown in Fig. 1b, in contrast to the ion source the neutralizer features a very small discharge chamber of 18 mm in inner diameter. The Xenon propellant pressure inside the chamber is controlled by a 4-mm-wide orifice diameter; with a conductance of the orifice below 1 sccm/torr. The inner pressure is kept at 5×10^{-3} to 1×10^{-2} torr for a Xenon mass flow rate of 0.5 to 2.0 sccm. A 4.2-GHz microwave is fed through a coaxial line followed by an L-shaped antenna, and the microwave transmission is tuned by a stub located outside the discharge chamber. The tip of the antenna is inserted into a magnetic field formed by front- and back-yokes and block magnets. If a strong magnetic field above the ECR condition is available, the compact magnetic flux tube in Fig. 1b works as a virtual cathode in the same manner as the ion source; the trapped electrons are energized and then actively ionize xenon atoms. With this type of antenna-plasma coupling, easy startup of the neutralizer and overdense plasma production was expected and was confirmed in the experimental results. Plasmas diffusing from the virtual cathode fill the discharge chamber, and a biasing voltage extracts electrons from the discharge chamber. In this context, the presence of an excessively strong magnetic field will hinder electron extraction; hence, the optimal strength of the magnetic field has to be selected.

C. Ion Optics

Flat, circular grids, 150 mm in diameter and 1 mm in thickness, were fabricated from a 30-cm-square Carbon/Carbon (C/C) panel.[11] A pitch-based carbon-fiber felt consisting of tangled continuous filaments of about 10 μm in diameter was selected. For additional strength and mechanical stability, a carbon matrix was deposited on the pitch-based fibers by a chemical-vapor-infiltration technique.[12] After the C/C composite was shaped into a thin plate, precise mechanical drilling was used to create grid holes. About 800 straight holes were drilled and located in a 3.5-mm pitch with ±0.02-mm accuracy. The hole diameters were different for each grid: 3.0 mm for the screen grid, 1.8 mm for the accelerator grid, and 2.4 mm for the decelerator grid. Spacing between the grids was kept at 0.35 mm for the accelerator-screen grids gap and 0.5 mm for the accelerator-decelerator grids gap. The C/C grid plates were mounted via ceramic spacers attached to an aluminum ring. The grids were separated from each other by these spacers. Their gaps were precisely adjusted when they were torqued to the ring. This fastened grid attachment increases the strength of the assembly and allows the grid-to-grid gap to be controlled to ±0.04-mm accuracy. The effective ion beam diameter is about 100 mm.

III. Experimental Apparatus

Using the just-mentioned EM thruster head, thruster performance and beam plasma profiles of the microwave ion thruster were measured. In addition, internal plasma profiles of both the ion source, Y-IV, and the neutralizer were obtained for an operation without beam extraction. Test facilities and procedures for these measurements are described here.

A. Test Facility for Performance Measurement

Electrical connections for both the thruster performance measurement and the beam plasma diagnostics are explained based on Fig. 1a. Because the screen grid was directly attached to the ion source without any electrical insulation, both the ion source and the screen grid were equipotentially biased to +1500 V with respect to ground. The current through the screen power supply corresponds to the extracted beam current plus the accelerator grid-current. The accelerator grid was set to −350 V, and the decelerator grid is equal to the engine's ground, which is usually connected to the space chamber. To neutralize the ion beam, a bias voltage of about −30 V was applied between the engine's ground and the neutralizer to form a plasma bridge. The neutralizer's bias voltage was controlled to supply the same amount of electron current as ion beam current. Because the biased components have to be electrically isolated from each other and from the engine's ground, the engine's mount, gas port, and microwave feed lines have to be isolated using ceramics, dc breaks, or gas isolators.

The entire thruster system was operated in a vacuum chamber[13] 2 m in diameter and 5 m in length, which was evacuated by cryogenic pumps, maintaining the pressure below 5×10^{-6} torr (for air) during thruster operation with mass flow rates of 2.4 sccm for the ion source and 0.5 sccm for the neutralizer. Before measurements were made, the thruster was continuously operated for more than an hour to reach a thermal equilibrium state.

For the purposes of performance evaluation, the ion production cost is defined as the input microwave power divided by the extracted ion current. Here the accelerator current, which should be subtracted from the ion current, was less than 1.0 mA and was therefore neglected. The reflected microwave power, typically less than 10% of the input power, was not subtracted for data analysis because the reflected power cannot be used and is simply wasted in the microwave circuit. The microwave power detectors, which were calibrated using an HP437B/8485 power meter, have an error range of 2%. This and the ambiguity of insertion loss associated with microwave connectors led to a total error in the ion production cost of about ±3%. In addition, the propellant utilization efficiency was calculated as the ratio of ion current to xenon feeding rate in equivalent amperes, with the latter controlled to within ±2% accuracy for a mass flow rate of 2 sccm. The background

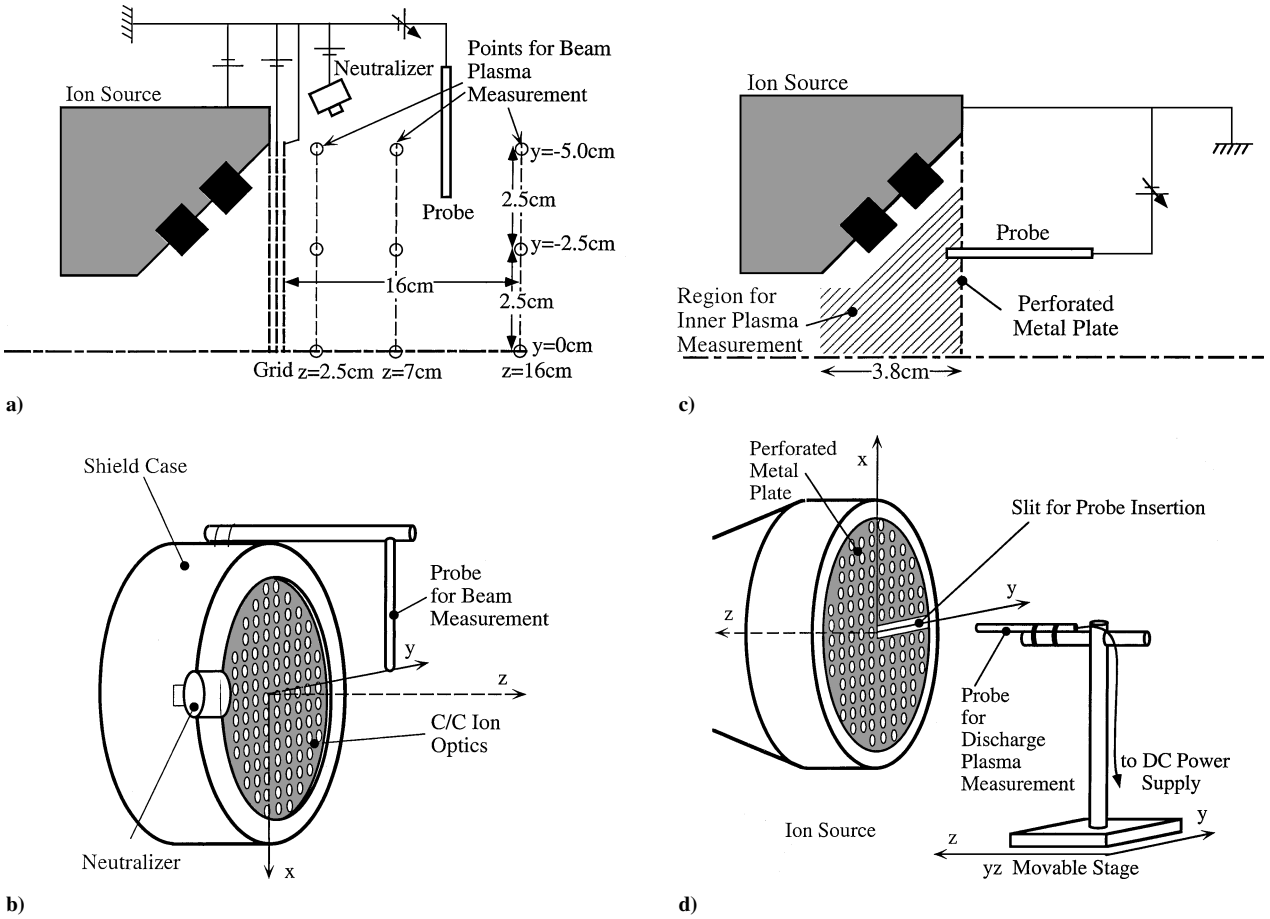

Fig. 2 Langmuir-probe scanning positions; a) and b) show the set for beam plasma measurement and c) and d) are for inner plasma measurement.

pressure was so low that its contribution to the mass flow rate was neglected.

B. Langmuir-Probe Measurement

A Langmuir-probe technique was employed to obtain plasma profiles of the beam (Figs. 2a and 2b) and the inside of the discharge chamber (Figs. 2c and 2d). If the probe surface is exposed to the beam plasma, the electric field of the probe cannot prevent penetration into the probe by the fast flowing plasma, and the corresponding fast ion current will dominate the probe current. To avoid this, a flat probe of 2 mm in diameter was placed perpendicularly to the ion beam axis. As shown in Fig. 3a, the probe consists of a tungsten rod inserted into a ceramic tube. Because only the end face of the tungsten rod is exposed to a plasma, fast beam ions flow parallel to the probe surface and the fast ions do not directly bombard the probe. With this configuration, the electrons and slow ions in the beam are captured by the biased probe but fast ions are not. To derive the properties of the beam plasma, the information on the electron current is used. In the configuration shown in Figs. 2a and 2b, however, beam divergence or a misaligned probe can cause the probe current to be affected by the incident ions and corresponding secondary electron emission. For a typical probe current of 200 μA at the electron saturation region, the beam ion current will reach 1 μA for a 5-deg inclined probe; corresponding secondary electron emission is about 1 μA, which will affect the electron saturation current by only 0.5%. In contrast, near the floating potential, the probe current is small and almost comparable to the ion current, and thus the probe characteristics can be affected by the fast ions. Such an effect is considered to be the major error source when the electron temperature is determined from the slope of the semilog plot of electron current, leading to an inaccuracy of $\pm 10\%$ in T_e for typical data observed in this experiment. Ambiguity also arises in evaluating V_s from a V-I curve; ± 2 V uncertainty of V_s corresponds to $\pm 30\%$ error in n_e.

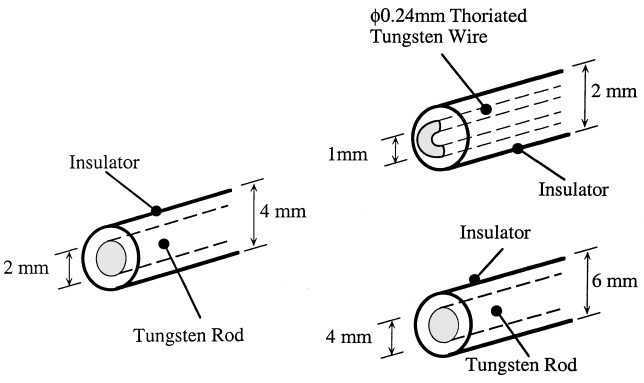

Fig. 3 Sketch of probes: a) Langmuir probe for beam plasma measurement and b) probes for discharge plasma measurement inside the ion source, with (upper) potential measurement, (lower) ion current measurement.

The effect of the magnetic field was considered to be negligible because of the weak magnetic strength, which was at most 10 Gauss in the beam.

In contrast, the effect of the magnetic field can not be neglected for plasma measurement within the discharge chamber; the typical B-field of the ECR magnet is 0.15 T. This strong field makes it almost impossible to convert the measured probe data to plasma properties. Hence, only two-dimensional images of the ion saturation current and floating/space potentials were considered. Difficulties in making probe measurements through the optics at high voltage were circumvented by placing a plate at the exit plane and inserting a probe through this plane (Fig. 2d).

Probes for the plasma measurements inside the discharge chamber are depicted in Fig. 3b. For floating potential V_f and space potential V_s measurement, a ring-shaped 0.24-mm-diam wire probe was used, while a plane probe of 4 mm diam was biased to -150 V for the ion saturation current measurement. RF compensation was not necessary because the electrons in the discharge chamber cannot respond to the fast electric field oscillation in the microwave range. This situation is different from that of rf discharges, in which the rf component of the plasma potential should be compensated.[14] Both the V_f and the V_s are measured using a digital meter that is accurate to ± 0.1 V, but the ambiguity of V_s reached ± 1 V when the V_s was determined from the emissive probe measurement. The error in the ion saturation current measurement was approximately 2% and was caused by secondary emission by ion bombardment. These probes were inserted through a slit in the perforated metal, as shown in Fig. 2d, and scanned every 4 mm to obtain a two-dimensional distribution. When these probes were inserted, the microwave reflected power was increased by about 5%, so that the plasma inside the discharge chamber was expected to be changed by about 5%.

C. Neutralizer Stand-Alone Test

For internal plasma characterization, the neutralizer was operated in a stand-alone configuration as shown in Fig. 4. In this test, the neutralizer was located in a small chamber measuring 0.3 m in diameter and 0.5 m in length, which was evacuated to below 1×10^{-5} torr using a rotary pump and a diffusion pump. A flat 1-mm-diam probe similar to that shown in Fig. 3a was used. For a dense plasma inside the neutralizer, the thin sheath model is applicable to the ion saturation region because $r_p/\lambda_D \gg 1$. For a 200-mA electron source with an internal wall area of 1500 mm^2, $n_e = 1.5 \times 10^{11}$ cm^{-3} can be deduced from the fact that the xenon ions flow into the wall of the neutralizer with the Bohm velocity, 5420 m/s for $V_s = 20$ V. Note that the electron source is operated at a temperature of around 400 K, for which no thermionic electron emission is expected. For $T_e = 10$ eV and $n_e = 1.5 \times 10^{11}$ cm^{-3}, $\lambda_D = 6.0 \times 10^{-5}$ m; accordingly, $r_p/\lambda_D = 8.3$. The Langmuir-probe measurement was conducted without biasing the neutralizer body. A comparison of biased and nonbiased neutralizer bodies shows no difference in plasma densities, but the temperatures of biased and nonbiased operations are different by a factor of 2. The higher electron temperature measured during the biased operation indicates the acceleration of the electrons. Because our interest is in characterizing the plasma density produced by the ECR discharge, we employed the result from the nonbiased neutralizer operation for the discharge plasma measurement.

For the preceding measurement scheme, two major error sources are considered: one is the effect of magnetic field, and the other is secondary electron emission by ion bombardment. The effect of the magnetic field is assessed for a magnetic field of about 0.01 T at the tip of the probe, where the electron Larmor radius is comparable to the probe radius of 0.5 mm. For a microwave input power above 4.8 W, the plasma density obtained from the ion saturation current is a factor of 1.1 to 1.5 smaller than the density calculated from the electron saturation current, which implies that the effect of the magnetic field on the probe characteristics is not negligible. In addition to the effect of the magnetic field, two other effects should be considered: 1) a 2% error is expected for the ion saturation current biased at -150 V because of the secondary emission current from the probe surface, and 2) ambiguity is associated with the space potential, ± 1 V, and corresponding $\pm 10\%$ error in the electron saturation current. The electron temperature, which is determined from the slope of the semilog plot of the probe current vs the probe voltage, is affected by the preceding uncertainty leading to an error of the electron temperature of as much as 60%. The n_e is affected by the error in T_e and by the ion saturation current, which can lead to an error range of $\pm$ 70%. For a microwave input power below 2.4 W, the plasma density obtained from the ion saturation current is a factor of 2–3 smaller than the density calculated from the electron saturation current. This is related to increased ambiguity because of plasma density below the cutoff density. At low plasma densities, secondary emission electrons will increase in the ion saturation region, and the thin sheath model almost breaks down. If the effect of the magnetic field is assumed to be the same as for the just-mentioned cases of microwaves above 4.8 W, the ambiguity of T_e for the case of a 2.4-W microwave is 70% and that for n_e is $\pm 80\%$.

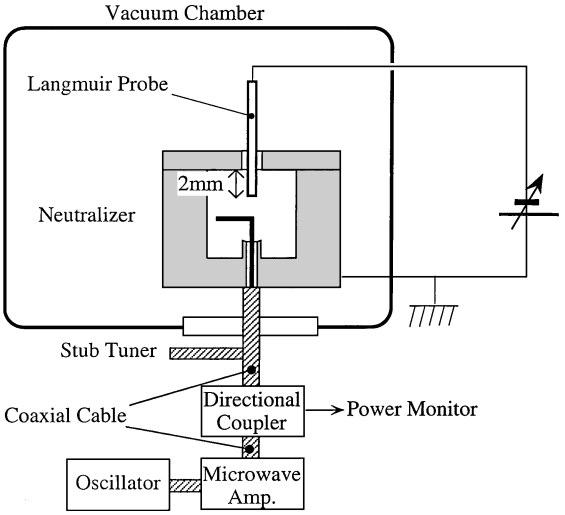

Fig. 4 Neutralizer stand-alone test.

IV. Experimental Results and Discussion

A. Thruster Performance

Figure 5 shows a typical performance curve of the ion source. An ion beam of 140 mA can be generated at 32-W microwave power and a mass flow rate of 2.4 sccm. This condition corresponds to an ion production cost of 230 A/W and a propellant utilization efficiency of 80%. The performance curve for a constant microwave power reveals the characteristics of the microwave ion source. Along the curve in Fig. 5, both the production cost and the utilization efficiency were improved when the mass flow rate was increased up to 2.25 sccm. This knee point located at 2.25 sccm corresponds to the best operational point, which enables both low ion production cost and high utilization efficiency. Further increasing the mass flow, however, drastically degrades utilization efficiency, which implies that the plasma production cannot be increased. The extra xenon atoms supplied are not used but instead leak out through the optics

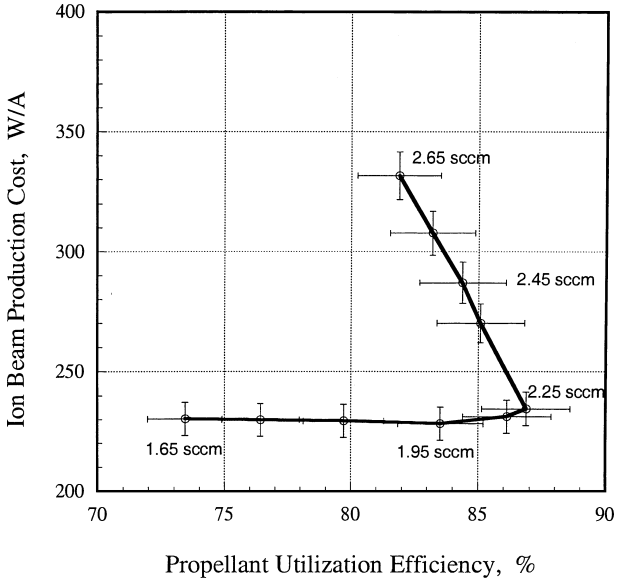

Fig. 5 Typical thruster performance for ion production (EM thruster, $P_f = 32$ W).

in the form of neutral gas. This reduced utilization efficiency for the large mass flow rates (and accordingly, for large internal pressures) strictly limits the operational range of the microwave ion source. Such a limit cannot be overcome even if the microwave power is further increased; instead, it was found that beam current was only a weak function of input microwave power above 32 W, so that the ion production cost was severely degraded for that operational range even at fixed mass flow rate.[1] These restrictions concerning both the inner pressure and the microwave power are attributed to the mechanism of the virtual cathode, which will be discussed later in this section.

The best thruster performance, 32 mN/kW, was measured at an input microwave power of 40 W (32 W for the ion source and 8 W for the neutralizer) and a beam power of 240 W. At this condition 8 mN was achieved with a thrust coefficient of 0.92 (mostly attributed to 10% doubly ionized xenon).[15] The system performance for the MUSES-C is somewhat worse, because of transmission line loss and limited microwave power generation efficiency. To introduce 40-W microwave power to the thruster, more than 70 W is required for the microwave amplifier.

B. Plasma Properties of the EM with Beam Extraction

Figure 6 shows beam plasma profiles near the engine. As a result of localized plasma production near the magnets, peaks were found at $r = \pm 2.5$ cm in the case of electron density, leading to a donut-shape beam profile. The central axis ($r = 0$ cm) corresponds to the position of the waveguide, where only limited plasma production is expected. This near-field profile flattens out further downstream. Near the neutralizer, which is located at $r = -6$ cm, the T_e is relatively high, which suggests that a large number of high energy bulk electrons were produced at the neutralizer by the neutralizer bias voltage.

Because there is no keeper electrode for the microwave neutralizer, extraction of electron current was conducted by biasing the neutralizer body with respect to the engine's ground. For this case, the biasing voltage was −23 V. The biasing voltage was inversely proportional to the distance of the neutralizer body from the ion beam. Considering this characteristic, the neutralizer should be located as close as possible to the ion beam, but not so close as to be intercepted by the ion beam, in order to avoid a large bias voltage that would lead to a reduced lifetime. The decelerator grid prevents low-energy ions produced by the neutralizer from bombarding the accelerator grid. The neutralizer operates in plume mode because of the inherently limited electron emission capability. This assertion is based on the internal plasma data that were obtained by the setup shown in Fig. 4 (without biasing its body) via Langmuir probes. The results are shown in Fig. 7; the neutralizer plasma density is large, achieving 10^{11}–10^{12} cm^{-3} for microwave powers above 4.8 W, while

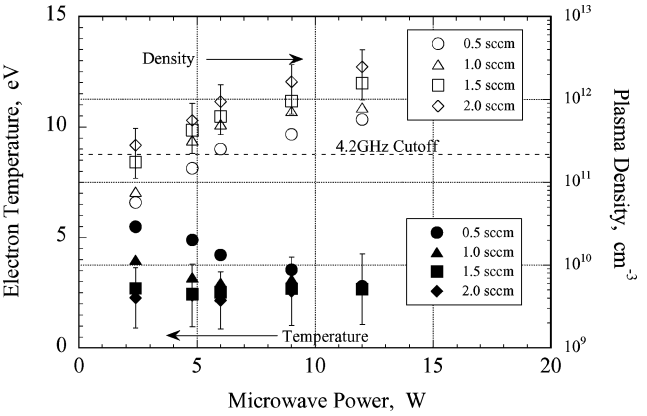

Fig. 7 Plasma density and electron temperature inside the neutralizer (EM, bias voltage was set to 0 V). Error bars were plotted only for 2 sccm.

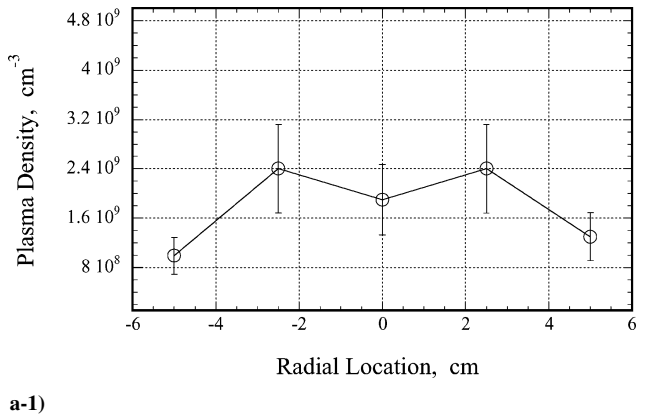

a-1)

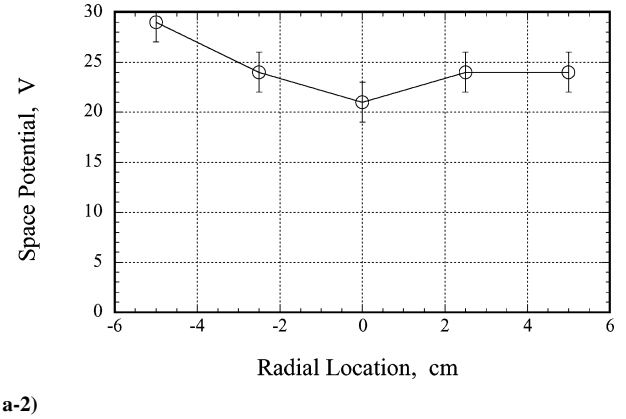

a-2)

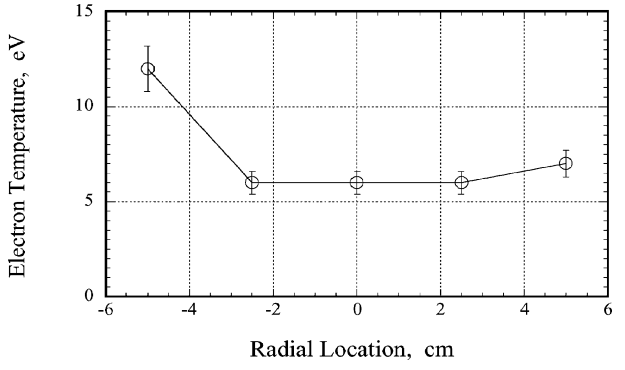

a-3)

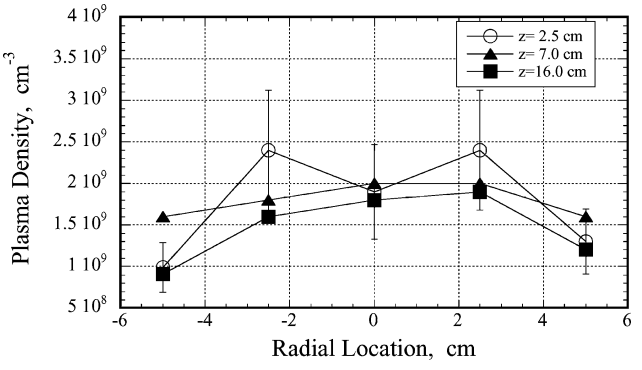

b)

Fig. 6 Beam plasma profile of EM thruster for $V_{sc} = 1.5$ kV, $V_{ac} = -300$ V, $V_{neut} = 23$ V, $I_b = 137$ mA, $\dot{m}_i = 2.3$ sccm, $\dot{m}_{neut} = 0.5$ sccm, $P_f = 32$ W, and $P_{neut} = 8$ W: a) radial distributions of plasma density (a-1), space potential (a-2), and electron temperature (a-3) at a distance of 2.5 cm from the decelerator grid; b) radial plasma profiles at various locations along the plume axis. For b) Fig. 6, error bars were plotted only for $z = 2.5$ cm.

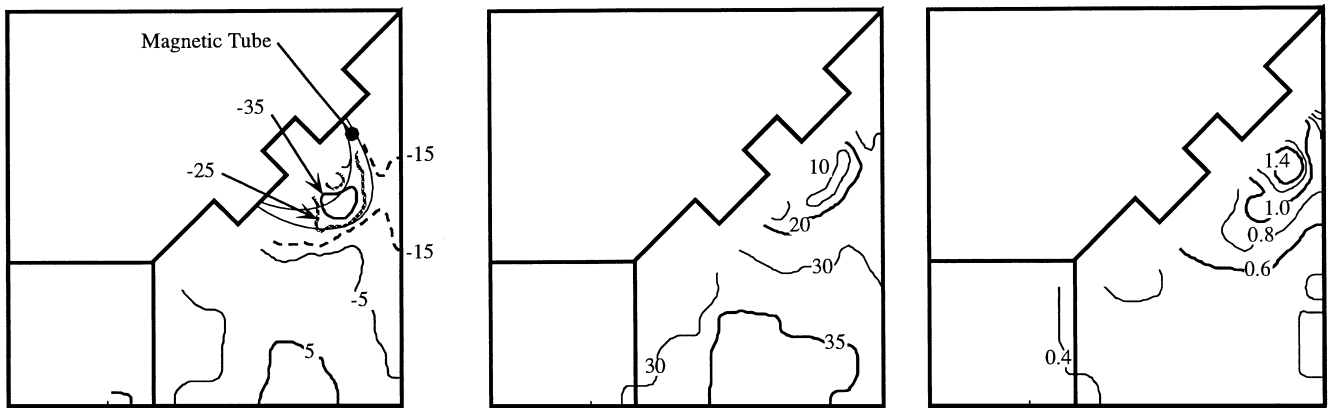

a) Floating potential, V **b) Plasma potential, V** **c) Ion saturation current, arbit**

Fig. 8 Ion saturation current, floating potential, and plasma potential profiles inside the thruster head ($P_f = 40$W, $\dot{m}_i = 1$ sccm (pressure inside the discharge chamber is 5.8×10^{-5} torr), Y-IV thruster head, without beam extraction).

the electron temperature remains relatively unchanged at around 3 eV. The plasma density inside the discharge chamber was far beyond the cutoff density of the 4.2 GHz microwave, 2×10^{11} cm^{-3}. For this overdense plasma, the penetration depth of the microwave emitted from the antenna, that is, the skin depth, is about 2 mm for a 10^{13} cm^{-3} plasma, and therefore the microwave does not propagate inside the discharge chamber but oscillates only near the surface of the antenna. In the same manner as in the ion source, the small magnetic flux tube inside the neutralizer corresponds to an ionization region, in which the high-energy electrons are trapped and ionize the background xenon atoms. By inserting an L-shaped microwave antenna into the ECR region, it is possible to directly oscillate the ECR region and to make a "cutoff-free" plasma.

The charge-exchange mechanism between the plasma and the chamber wall of the neutralizer is noteworthy. Considering that the temperature of the microwave neutralizer in operation is about 100°C, thermionic electron production is negligible. Under such conditions, the neutralizer collects ions at the surface of the inner body; for this charge exchange, only singly charged ions are of importance, because other contributions, such as doubly charged xenon ions or metastable atoms, are negligible.[16] With the just-mentioned charge-exchange mechanism, in spite of efficient plasma production that exceeds the cutoff density of the microwave, the electron emission current for a given input power is still small compared to thermionic emission by the hollow cathode.

Aside from performance, issues of the lifetime of the neutralizer are also of interest. For the microwave discharge, which requires neither thermionic material nor a heater to start up the discharge, ion bombardment into the body and the corresponding erosion of the body are considered to be the major wear mechanisms. Hence, the biasing voltage should be controlled so as not to exceed the sputtering threshold, above which the erosion by ion bombardment is not negligible. The neutralizer with the EM thruster head was tested for endurance using an input microwave power of 8 W and a mass flow rate of 0.5 sccm. With a biasing voltage of about −23 V with respect to ground and the space potential of the beam 25 V, the neutralizer body is set to about 48 V lower than the potential of the ion beam. Although this biasing voltage is higher than the sputtering threshold of molybdenum, 27 V, only a small amount of erosion was observed during endurance tests.[17] Accelerated erosion tests, in which the neutralizer body was eroded in proportion to both current and voltage, were also performed, and the longevity was confirmed for the bias voltage of 49 V.

C. Simulated Plasma Profile of Y-IV Without Beam Extraction

The peak ion current density obtained for the thruster was 1.8 mA/cm^2, which is a factor of 2–3 smaller than that of dc discharge thrusters.[18,19] Increases in the microwave power resulted in increases in the ion production cost. Likewise, further increasing the mass flow rate (or, equivalently, the internal xenon gas pressure) abruptly degraded the utilization efficiency and did not result in an increase in beam current. These limitations, as indicated before, might be inherent to the design of the microwave discharge ion source, and might considerably restrict the operational range of the thruster. Using the Y-IV thruster head, the internal plasma properties were acquired in order to obtain the correlation between the operational parameters and the plasma profiles. Along with the data, microwave-to-plasma coupling inside the ion source is discussed here.

Figure 8 shows a plasma profile inside the discharge chamber. Note that the pressure inside the discharge chamber was adjusted to 5.8×10^{-5} torr, which simulates ion beam extraction from the plasma. The pressure inside the discharge chamber p_2 was calculated from the mass flow rate following the equation:

$$p_2 - p_1 = \dot{m}_{\mathrm{sim}}/C \tag{2}$$

where $\dot{m}_{\mathrm{sim}}$ is selected as

$$\dot{m}_{\mathrm{sim}} = \dot{m}_i(1 - \eta) \tag{3}$$

to simulate the beam extraction with a mass flow rate and a utilization efficiency. Although this selection does not necessarily simulate the beam extraction, the objective of this measurement is not to strictly simulate the beam extraction, but to study how the plasma profile is affected by changes in pressure. Therefore, a pressure near the beam extraction condition was selected. As the figures show, large ion current and large negative floating potential were observed near the magnet. The latter negative floating potential corresponds to trapped primary electrons, whereas the peak of the ion current implies that plasmas are actively produced in the same region. This region is located at the center of one of the magnetic flux tubes, as is depicted by solid lines in Fig. 8a, demonstrating plasma production based on a virtual cathode. In contrast to the localized plasma profile, the plasma potential in the discharge chamber stayed at a moderate positive value throughout the discharge chamber. Aside from the just-mentioned plasma potential, floating potential, and ion saturation current distributions, high-energy electron measurements are very important to reveal the mechanism behind the plasma production process. The presence of such primary electrons was confirmed only optically. In Ref. 20, we used Xe II lines to identify electron energies because an emission line appears only when electrons above an excitation energy threshold exist. For Xe II, these thresholds correspond to 20–30 eV; hence, high-energy electrons beyond 20–30 eV were successfully observed. However, the measured emission intensity does not give an electron energy distribution function but rather gives its integration with respect to energy.[21] Thus, quantitative estimation of energetic electron components is impossible by this method. When helium is mixed into the discharge (excitation threshold of helium is 70 eV), the He-II line was observed in addition to the Xe lines, indicating the presence of energetic electrons.

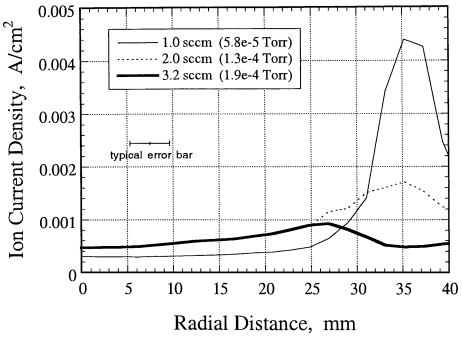

Fig. 9 Dependence of ion saturation current profile on discharge chamber pressure ($P_f = 40$ W, Y-IV thruster head, without beam extraction). Error source is related to position uncertainty.

Observation of these emission lines qualitatively indicates that electrons of several tens of eV are produced in the magnetic flux tube and play an important role in the ionization processes. We have not so far succeeded in detecting high-energy electrons by the probe method, so that the resolution of high-energy electrons is limited. A preliminary test using the Druvesteyn method showed no evidence of tail electrons within the accuracy of the probe measurement. It is therefore expected that there is only a small population of such high-energy electrons, which are required to ionize the gas.

The dependence of ion source performance on the mass flow rate (Fig. 5) suggests that the plasma profile will be considerably influenced by the pressure inside the ion source as calculated by Eq. (2). The effect of pressure on the plasma profiles is clearly seen in Fig. 9, in which the horizontal error bar is associated with positioning uncertainty. For the low-pressure case (5.8×10^{-5} torr), the ion current density has a peak high density approximately 35 mm off the axis. In contrast, increasing the pressure to 1.3×10^{-4} torr drastically reduces the ion current, which leads to a decrease in the total beam current. The large discrepancy between the plasma profiles of the low-pressure case (5.8×10^{-5} torr) and the high-pressure case (1.3×10^{-4} torr) is related to collisional phenomena of electrons in the virtual cathode. To realize efficient plasma production in the virtual cathode, low-energy electrons must be energized to high-energy states above the ionization threshold without being disturbed by collisional and/or diffusive processes. If a large number of high-energy electrons is produced and the electron energy distribution deviates along a Maxwellian distribution, the magnetic flux tube can supply high-energy electrons, and the flux tube really works as the virtual cathode. This is realized when electrons are continuously energized by the ECR process without being disturbed by a collisional process. To consider such a process, various collision frequencies inside the ion source were calculated and then compared for a low-energy electron. We take into account, for example, a 10-eV electron, for which direct ionization is negligible. The frequency of the collective long-range Spitzer collision for 10-eV electron is estimated as $\nu_{ei} = 2 \times 10^5$ Hz, if the plasma density is assumed to be the cutoff density (2×10^{11} cm^{-3}). Other frequencies depend on the discharge chamber pressure; at low pressure 10^{-4} torr, $\nu_{en} = 2 \times 10^6$, and $\nu_{en} = 2 \times 10^7$ Hz for 10^{-3} torr. These collision frequencies are compared with the frequency of energy gain by ECR, ν_{ECR}, which is easily derived based on Fig. 10. If the electric field in the discharge chamber is not strong, we can assume that the magnetic moment μ will increase only slightly when passing the ECR line once. Applying the conservation of magnetic moment $\mu \approx$ const to an electron in the mirror magnet, it is apparent that the electron has four chances to cross the ECR line during each bouncing movement. Hence,

$$\nu_{ECR} = 1/(\tau_{bounce}/4)$$

The time elapsed during a bouncing motion is derived by integrating $u_{//}$ along the magnetic field,

$$\tau_{bounce} = 4 \int_0^{\ell'/2} \frac{d\ell'}{u_{//}} \tag{4}$$

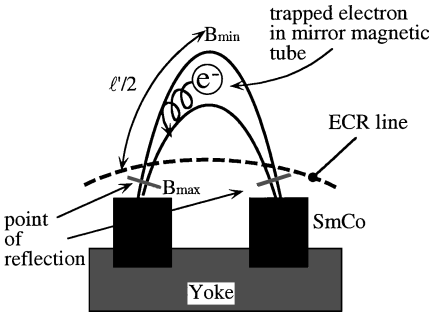

Fig. 10 Electron motion in the mirror magnetic field.

where $u_{//}$ is expressed as

$$u_{//} = [(2/m_e)(W_{tot} - \mu B)]^{\frac{1}{2}} \tag{5}$$

If approximation

$$\frac{dB}{d\ell} \approx \frac{B_{max} - B_{min}}{\ell'/2} \tag{6}$$

and the conservation of particle energy $W_{tot} =$ const. are valid; ν_{ECR} is derived using Eqs. (4) and (5):

$$\nu_{ECR} = \frac{1}{\tau_{bounce}/4} = \frac{\sqrt{2}(B_{max} - B_{min})\mu}{\ell'[m_e(W_{tot} - \mu B_{min})]^{\frac{1}{2}}} \tag{7}$$

With Eq. (7), $\nu_{ECR} = 3 \times 10^7$ Hz is obtained for $W_{tot} = 10$ eV, $\mu = 0.8 \times 10^{-17}$ J/T, $B_{max} = 0.2$ T, $B_{min} = 0.1$ T, and $\ell' = 0.05$ m. In case W_{tot} and μ are not conserved, that is, a large-energy gain is expected for a passage across the ECR line, Eq. (4) cannot be easily integrated, but ν_{ECR} will be numerically given. Even for this case, $u_{//}$ is not very large, but $u_{\perp}$ will increase, and the order of magnitude of ν_{ECR} will be close to the calculated value.

To sustain a plasma, the virtual cathode must be populated with many high-energy electrons that can ionize the background neutrals. If $\nu_{en} \geq \nu_{ECR}$, during the bouncing movement in the magnetic tube an electron will lose its energy before reaching the ECR zone, so that the total number of high-energy electrons will not increase. In contrast, if $\nu_{en} < \nu_{ECR}$, an electron of 10 eV can acquire extra energy by crossing the ECR zone before colliding with a neutral particle. Such an energy-duplicating process becomes possible for a low pressure of 1×10^{-4} torr; under this condition, the energized electron has a chance to reach another ECR zone before colliding with a neutral gas and losing its energy. With such a process, primary electrons above the ionization energy are produced. These tail electrons are not depleted by the Coulomb collision because of the small electron–electron collision frequency, but are rather depleted by collision with a neutral atom that will directly produce another electron–ion pair. For a higher pressure, on the order of 10^{-3} torr, the just-mentioned enhanced plasma production is prohibited because the electron loses its energy in collision with an atom before receiving extra energy. On the other hand, for a much lower pressure, below 10^{-4} torr, the very low rate of collision with neutrals drives the electrons to overheat, and the corresponding large electron loss to the wall degrades plasma production cost. This discussion suggests that there is an optimum pressure for the microwave discharge ion thruster for a specific input power.

For efficient plasma production, in addition to the just-mentioned collisional condition for increasing electron energy, the microwave power must reach the resonant line before being reflected. This is sometimes problematic because wave propagation can be prohibited by a high-density plasma near the cutoff. Wave accessibility and resonance are explained based on Fig. 11, in which the propagation of a cold plasma wave is summarized following the Clemmow–Mullaly–Allis (CMA) diagram.[22] The CMA diagram shows a plot of ω_c/ω against ω_p^2/ω^2 or, equivalently, a plot of magnetic field against density. For a given frequency ω, any experimental situation characterized by ω_p and ω_c is denoted by a point on the graph.

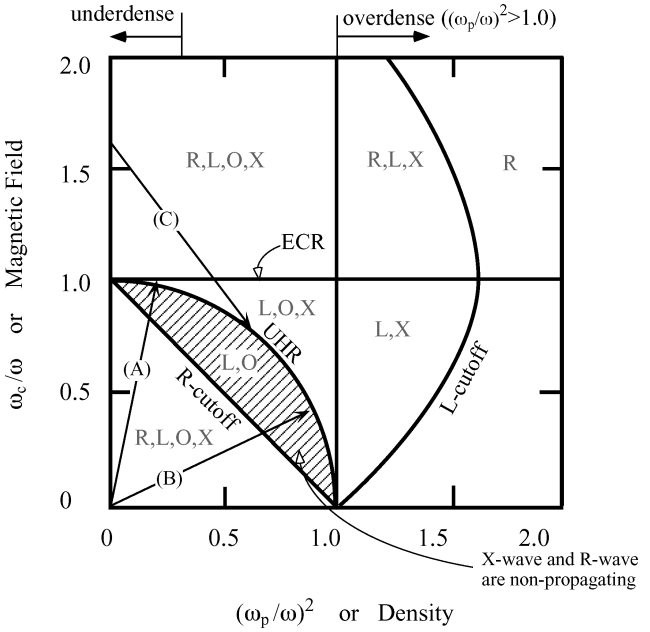

Fig. 11 Expected microwave propagation and cutoff regions inside the ion source; regions are bounded by the cutoff and resonant lines, and in each region only the waves in gray characters can propagate. For example, in the shaded region the L- and O-wave can propagate, but the R- and X-wave are nonpropagating.

Waves propagating in the B-field are divided into two groups: 1) those that propagate along the B-field and 2) those that propagate perpendicularly to the B-field. In the case of the wave propagation strictly along the B-field, if the electric field vector rotates in the same direction as the electrons rotate in the B-field, the wave is called an R-wave (right-hand circularly polarized wave). Similarly, if the electric field vector rotates in the other direction, the wave is referred to as an L-wave (left-hand circularly polarized wave). Of the two, only the R-wave is resonantly absorbed by electrons at the ECR frequency and is thus useful for ECR, as was pointed out in introduction. If the R-wave reaches the ECR line, efficient wave–particle interaction is possible. In the case of the ion source, however, if the R-wave is launched from the low B-field side, for example, following path A in Fig. 11, then the wave is blocked at the R-cutoff, and the accessibility breaks down. In this case, the R-wave will penetrate into the ECR in an evanescent mode, in which the penetrating wave will tunnel through the abandoned zone between the R-cutoff and the ECR along path A. This is, however, not difficult, because the discharge chamber size is very compact, only 10 cm in diameter, which is below the wavelength of 70 mm. Accordingly, the length between the R-cutoff and the ECR is short, and the wave is partially transmitted through the abandoned zone without being totally reflected. This situation is different in the case of a higher electron density. For wave propagation along line B, the distance between the ECR and the R-cutoff increases. Therefore only a small amount of the R-wave tunnels through the abandoned zone, and most of it is reflected in the case of overdense plasma. This is one of the reasons that a plasma source of this type shows a limited plasma density, and hence beam current, even if the microwave power is increased.

There is another mechanism of wave propagation and energy absorption in addition to the R-wave. Ordinary waves (O-wave) and extraordinary waves (X-wave) can propagate perpendicular to the B-field. In the case of the O-wave, the electric field vector of the wave is parallel to the B-field, whereas for the X-wave the electric field vector of the wave is perpendicularly to the B-field. As in the case of the ECR frequency for the R-wave, the upper hybrid resonance $\omega_{\mathrm{UH}} = \sqrt{(\omega_p^2 + \omega_c^2)}$ corresponds to the resonance for the X-wave. Unfortunately, access to the UHR frequency is prohibited by the R-cutoff when the X-wave is launched from the weak field side along path A. This accessibility difficulty can be overcome because the X-wave can tunnel through the R-cutoff. To overcome the large reflected microwave power, threfore, only the X-wave should be used. However, in realistic cases the wave propagates neither strictly parallel nor strictly perpendicular to the B-field. Accordingly, for a wave launch from the high B-field side the R-wave and the X-wave are rather difficult to distinguish. Such a case will apply to the small discharge chamber of the microwave ion source, in which the wave is launched neither as purely X-wave nor as R-wave.

The mechanism of resonant wave absorption for the X-wave by way of the UHR line is not introduced in the cold plasma theory. The resonant coupling by UHR in a dense plasma near the cutoff or even in an overdense plasma has been intensively discussed with respect to fusion plasmas[23] and process plasmas,[24] where very strong wave-plasma coupling is usually expected, especially as a form, for example, of wave conversion to an intense electrostatic wave, followed by strong nonlinear absorption processes. In spite of these UHR wave absorption mechanisms for high-density plasmas, the accessibility difficulty also arises for UHR as a result of the O-mode propagation[4]; in the small microwave ion engine, the O- and the X-waves cannot be separated but rather coexist in the discharge chamber. Only the X-mode is expected to be strongly absorbed on the UHR line, and the O-mode is reflected when the plasma exceeds the cutoff density. In addition to wave reflection at the R-cutoff, this is another reason that plasma sources of this type show a limited plasma density.

Of course, there is a possibility that some of the O-, L-, and R-waves will penetrate into the chamber and then undergo reflection at the wall followed by mode conversion into the X-wave and corresponding resonant wave absorption. In these cases, however, most of the O-, L-, and R-waves are expected to be unresonantly damped or reflected back to the matching circuit for the case of the overdense plasma. This wave-plasma coupling difficulty restricts the operation of the ion source. For this wave launcher design, that is, from the low-field side wave injection, it is therefore only below the cutoff density, that is, at low microwave input power, that efficient wave-to-plasma power coupling is realized.

Even though the UHR mechanism is considered important in enhancing plasma production near the cutoff, the magnetic field configuration has to be changed for that purpose, which will be explained in the following. The UHR line, $\omega_{\mathrm{UH}} = \sqrt{(\omega_p^2 + \omega_c^2)}$, changes its location as the electron density approaches the cutoff. After the UHR line is drastically shifted toward the low-B-field side for larger electron densities, there is no intersection between the magnetic tube and the UHR line, which means electrons that absorb energy on the UHR line have no chance to successively acquire extra energy but they will move around the discharge chamber without being trapped in the magnetic tube. In this case, there is no virtual cathode, and a typical electron can acquire energy at the UHR line only once before a collision with a neutral particle. If the configuration of the weaker part of the B-field is arranged for the UHR, further improvement is possible for the plasma production near the cutoff. Restriction of the O-, R-, and L-wave propagations remains, however, and is considered to deteriorate the wave-to-plasma coupling, thus degrading ion production cost near the cutoff. Note again that the use of the small discharge chamber as the ion source prohibits separating the X-wave from others, and only the X-wave can be absorbed by the UHR mechanism. Because the pure X-wave from the high-field side cannot be used, for example, along line C, launch by a wave guide suffers from the accessibility difficulty. If an overdense plasma is preferred in order to obtain a larger ion beam density, a compact antenna-type launcher like that used for the neutralizer, with an antenna directly inserted in to an overdense plasma, seems to be the only way to overcome the accessibility difficulty.

V. Conclusions

From the characterization of a 10-cm-diam microwave discharge ion thruster, it was found that internal plasma, and hence the beam plasma, are severely affected by the xenon gas pressure as well as the microwave input power. For an ion source design consisting of ring magnets into which the waveguide launches 4.2-GHz microwaves, a possible optimized condition for both parameters showed an ion

beam current of 140 mA for a microwave power of 32 W, which resulted in 8-mN thrust at an ion production cost of 230 W/A. This relatively small thrust density compared to that of a dc discharge thruster indicates different thruster scaling, which was optimized for a low plasma density inside the discharge chamber. For that parameter, microwave power coupling to the electron and plasma generation by these primary electrons are both conducted ideally, and the plasma showed a strong peak near the ring magnet, where ECR wave-plasma coupling resulted in a localized plasma generation. Although the preceding low-cost ion source was obtained, for the current launching mechanism of the microwave from the low-field side it is impossible to exceed the cutoff density in a low-cost way because there are some wave components that cannot penetrate into the cutoff plasma and reflect back to the microwave power source, which will degrade the ion production cost. In contrast to the ion source, the neutralizer plasma easily exceeds the cutoff, by the direct insertion of the tmicrowave antenna into the magnetic field.

Acknowledgments

The authors gratefully acknowledge the contribution of their colleagues at the Institute of Space and Astronautical Science: (ISAS) Yukio Shimizu, Kazutaka Nishiyama, Shin Satori (currently, Hokkaido Institute of Technology), and Yoshinori Nakayama (currently, National Defense Academy). In addition, the authors wish to thank the members of the MUSES-C project at ISAS, NEC TOSHIBA Space Systems, Ltd., and Mitsubishi Heavy Industries, Ltd., for their great support and for the fabrication of the microwave ion thruster system.

References

[1]Kuninaka, H., and Satori, S., "Development and Demonstration of a Cathodeless Electron Cyclotron Resonance Ion Thruster," *Journal of Propulsion and Power*, Vol. 14, No. 6, 1998, pp. 1022–1026.

[2]Kawaguchi, J., Uesugi, K., and Fujiwara, A., "The MUSES-C Mission for the Sample and Return—Its Technology Development Status and Readiness," *Acta Astronautica*, Vol. 52, No. 2, 2003, pp. 117–123.

[3]Kuninaka, H., Nishiyama, K., Shimizu, Y., and Toki, K., "Flight Operation of Microwave Discharge Ion Engines on HAYABUSA (MUSES-C)," AIAA Paper 2003-5289, July 2003.

[4]Goede, H., "30-cm Electron Cyclotron Plasma Generator," *Journal of Spacecraft and Rockets*, Vol. 24, No. 5, 1987, pp. 437–443.

[5]Kuninaka, H., Hiroe, N., Kitaoka, K., Ishikawa, Y., Nishiyama, K., and Horiuchi, Y., "Development of Ion Thruster System for Interplanetary Missions," *Proceedings of the 23rd International Electric Propulsion Conference*, Vol. 3, The Electric Rocket Propulsion Society, 1993, pp. 1805–1809.

[6]Ichimura, S., "Microwave Discharge Ion Thruster," M.S. Thesis, Univ. of Tokyo, Dept. of Aeronautics and Astronautics, Japan, March 1992 (in Japanese).

[7]Kuninaka, H., Ichimura, S., Kuriki, K., and Horiuchi, Y., "Ion Thruster with Electron Cyclotron Resonance Microwave Discharge," *Proceedings of the 18th International Symposium on Space Technology and Science*, Vol. 1, edited by H. Hirosawa, SANBI Printing Co., Tokyo, Japan, 1992, pp. 341–345.

[8]Nishiyama, K., Satori, S., Kuninaka, H., Kuriki, K., and Arakawa, Y., "Plasma Diagnostics Inside a Microwave Discharge Ion Thruster," *Proceedings of the 25th International Electric Propulsion Conference*, Vol. 1, The Electric Rocket Propulsion Society, 1997, pp. 371–378.

[9]Satori, S., Nishiyama, K., Kuninaka, H., and Kuriki, K., "Electron Cyclotron Resonance Ion Source for Ion Thruster," *Japanese Journal of Applied Physics*, Vol. 35, No. 1A, 1996, pp. 274, 275.

[10]Kuninaka, H., Satori, S., and Horiuchi, Y., "Continuous Operation Test of Microwave Discharge Ion Thruster System," AIAA Paper 95-3070, July 1995.

[11]Funaki, I., Kuninaka, H., Shimizu, Y., Toki, K., Nishiyama, K., and Horiuchi, Y., "Verification Tests of Carbon-Carbon Composite Grids for Microwave Discharge Ion Thruster," *Journal of Propulsion and Power*, Vol. 18, No. 1, 2002, pp. 169–175.

[12]Buckley, J. D., "Carbon-Carbon, An Overview," *Ceramics Bulletin*, Vol. 67, No. 2, 1988, pp. 364–368.

[13]Kuninaka, H., Funaki, I., Shimizu, Y., and Toki, K., "Endurance Test Facility and Test Status of Microwave Discharge Ion Thruster," *Proceedings of the 21st International Symposium on Space Technology and Science*, Vol. 1, edited by K. Vesugi, SANBI Printing Co., Tokyo, Japan, 1998, pp. 318–323.

[14]Godyak, V. A., Piejak, R. B., and Alexandrovich, B. M., "Measurements of Electron Energy Distribution in Low-Pressure RF Discharges," *Plasma Sources Science and Technology*, Vol. 1, 1992, pp. 36–58.

[15]Ohtaki, M., "Beam Diagnostics of a Microwave Ion Engine," M.S. Thesis, Nihon Univ., Dept. of Aerospace Engineering, Tokyo, Japan, March 1997 (in Japanese).

[16]Onodera, N., Takegahara, H., Nishiyama, K., Funaki, I., and Kuninaka, H., "Electron Emission Mechanism of Microwave Discharge Neutralizer," *Proceedings of the 26th International Electric Propulsion Conference*, Vol. 2, The Japan Society for Aeronautical and Space Sciences,Tokyo, Japan, 1999, pp. 902–909.

[17]Kuninaka, H., Funaki, I., Nishiyama, K., Shimizu, Y., and Toki, K., "Result of 18,000-hour Endurance Test on Microwave Discharge Ion Thruster Engineering Model," AIAA Paper 2000-3276, July 2000.

[18]Carruth, M. R., Jr., "A Review of Studies on Ion Thruster Beam and Charge-Exchange Plasmas," AIAA Paper 82-1944, Nov. 1982.

[19]Boer, P. C. T., "Electric Probe Measurements in the Plume of an Ion Thruster," *Journal of Propulsion and Power*, Vol. 12, No. 1, 1996, pp. 95–104.

[20]Funaki, I., Satori, S., Kuninaka, H., and Toki, K., "Plasma Diagnostics and Numerical Modeling of a Microwave Ion Engine," AIAA Paper 98-3341, July 1998.

[21]Sugai, H., Toyoda, H., Nakano, K., and Isomura, N., "A Biased Optical Probe Method for Measurements of Electron Energy Distribution in a Plasma," *Plasma Sources Science and Tehnology*, Vol. 4, No. 3, 1995, pp. 366–372.

[22]Stix, T. H., *Waves in Plasma*, Chap. 2, American Inst. of Physics, Springer-Verlag, New York, 1992.

[23]Batchelor, D. B., Goldfinger, R. C., and Weitzner, H., "Ray Tracing near the Electron Cyclotron Frequency with Application to EBT," *IEEE Transactions on Plasma Science*, Vol. PS-8, No. 2, 1980, pp. 78–89.

[24]Veerasingam, R., Campbell, R. B., Klevans, E. H., and McGrath, R. T., "Ray Tracing Calculations of ECR Absorption in Plasma Etching and Deposition Devices," *Plasma Sources Science and Technology*, Vol. 3, No. 2, 1994, pp. 142–153.